Ventilation of the North Atlantic and North Pacific: Subduction Versus Obduction*

BO QIU

Department of Oceanography, University of Hawaii at Manoa, Honolulu, Hawaii

RUI XIN HUANG

Department of Oceanography, University of Hawaii at Manoa, Honolulu, Hawaii,
Department of Physical Oceanography, Woods Hole Oceanographic Institution, Woods Hole, Massachusetts

(Manuscript received 27 June 1994, in final form 20 March 1995)

ABSTRACT

Ventilation in the North Atlantic and North Pacific is examined by analyzing the Levitus climatological data and the Hellerman and Rosenstein wind stress data. Ventilation between the permanent pycnocline and the overlying seasonal pycnocline and mixed layer consists of two physical processes: subduction and obduction. Subduction takes place mainly in the subtropical basin where surface water is irreversibly transferred into the permanent pycnocline below. Obduction takes place in the subpolar basin where water from the permanent pycnocline is irreversibly transferred into the mixed layer above.

Ventilation in the North Atlantic and North Pacific can be classified into four physically different regions: the subductive region, the obductive region, the ambiductive region where both subduction and obduction take place, and the insulated region where neither subduction nor obduction occurs. Although the total subduction rates in these two oceans are comparable, the total obduction rates are considerably different. In the North Atlantic, obduction is strong (23.5 Sv), consistent with the notion of the fast thermohaline circulation and the relatively short renewal time of the subpolar water masses in the Atlantic basin. Obduction is weak in the North Pacific (7.8 Sv); this is consistent with the sluggish thermohaline circulation and the slower renewal process of the subpolar water masses there. Accordingly, the water mass renewal time based on the subduction/obduction rate is calculated and compared with previous estimations.

1. Introduction

Motion in the upper ocean, which consists of the mixed layer and the seasonal and permanent pycnoclines, is dominated by wind forcing. Since the Ekman flux divergence is the primary driving force, a key parameter commonly used in describing the upper-ocean circulation has been the Ekman pumping rate. In order to understand water mass formation and climate variability, however, it is important to know the water mass exchange rate between the surface layer and the permanent pycnocline below.

Iselin (1939) proposed the first conceptual model of water mass formation. According to his model, Ekman pumping in late winter forces water to cross the base of the Ekman layer and to flow along isopycnals thereafter. Since the physical processes involved in the seasonal cycle are rather complicated, it was unclear why the subsurface ocean selects only the late winter properties of the surface water. By analyzing hydrographic data in the North Atlantic, Stommel (1979) studied the physical processes involved in the selection. He showed that if one is to examine the geostrophic region below the seasonal pycnocline, the complicated seasonal cycle can be avoided by simply taking a snapshot of the mixed layer parameters, such as the mixed layer depth and density, in late winter. So far, most of the ideal-fluid pycnocline models and subduction rate diagnoses from climatological data are based upon this hypothesis (aka the Stommel demon; see Williams et al. 1994).

Woods (1985) emphasized the importance of the dynamic role of the mixed layer, especially the horizontal gradient of the mixed layer depth and its seasonal cycle. Figure 1 shows a modified version of his schematic picture, illustrating the water mass movement. The upper ocean is divided vertically into four layers: the Ekman layer, the mixed layer, the seasonal pycnocline, and the permanent pycnocline. For simplicity, density is assumed vertically homogenized within the mixed layer, and flows below the mixed layer are assumed

* School of Ocean and Earth Science and Technology Contribution Number 3908. Woods Hole Oceanographic Institution Contribution Number 8942.

Corresponding author address: Dr. Bo Qiu, Department of Oceanography, School of Ocean and Earth Science and Technology, University of Hawaii at Manoa, Honolulu, HI 96822.

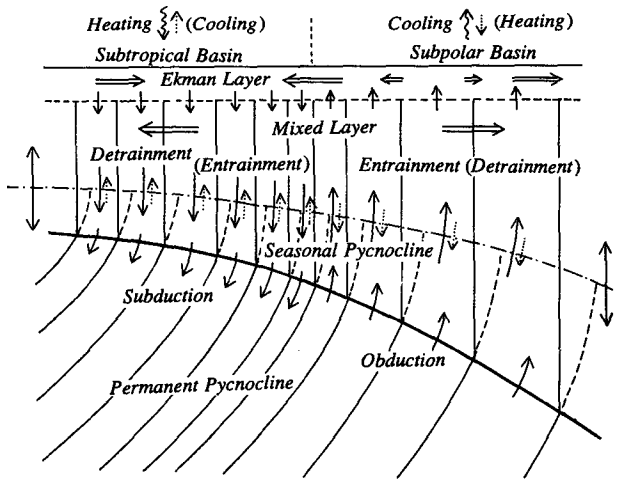

FIG. 1. Schematic illustrating the subduction and obduction processes. Within the permanent and seasonal pycnoclines, stratification is assumed to be time independent and motions geostrophic. The interface between the mixed layer and the seasonal pycnocline (depicted by the dotted–dashed line) moves up and down annually, as depicted by alternating arrows. Detrainment (entrainment) takes place at the base of the mixed layer. Only a part of the detrained water eventually enters the permanent pycnocline and this is termed subduction. Similarly, only a part of the entrained water actually originates from the permanent pycnocline, which is termed obduction.

geostrophic. Mass fluxes across the base of the mixed layer are conventionally termed "detrainment" or "entrainment," depending on the sign of the flux.

For studies of the oceanic general circulation and climate, a more important quantity is the annual mass flux entering or leaving the permanent pycnocline (Fig. 1). In this study, subduction is used to indicate the mass fluxes entering the permanent pycnocline from the overlying seasonal pycnocline. If there were no seasonal cycle, the base of the mixed layer would be fixed and there would be no seasonal pycnocline; in this case, the detrainment rate for waters leaving the mixed layer would equal the subduction rate.

The existence of the seasonal cycle, however, alters this balance significantly. The seasonal pycnocline plays the role of a buffer between the mixed layer and the permanent pycnocline. The subduction rate is quite different from the detrainment rate because each represents mass flux crossing a different interface. Assuming the flow in the permanent pycnocline is quasi-steady, subduction across the upper surface of the pycnocline takes place year round, as depicted in Fig. 2. In the subtropical basin, the seasonal cycle prevails, and detrainment/entrainment takes place alternately. Since the annual excursion of the mixed layer depth greatly exceeds the Ekman pumping term, the detrainment (entrainment) rate is primarily controlled by the rapid mixed layer shoaling (deepening) due to surface buoyancy gain (loss). As a result, the instantaneous detrainment rate can greatly exceed the subduction rate. It is, thus, preferable to discuss the annually averaged amount of effective detrainment (which will be defined more accurately below) than the instantaneous detrainment rate.

Although mixed layer detrainment takes place for a long period of the seasonal cycle, only a part of this period can be linked to subduction (Stommel 1979; Woods 1985; Cushman-Roisin 1987). In the interior subtropical basin, mixed layer detrainment starts in spring when the surface buoyancy forcing changes sign. As the water is detrained into the seasonal pycnocline, it flows geostrophically as the diapycnal mixing and turbulent stresses are negligible (Woods 1985). Notice that only a fraction of this detrained water, as depicted in Fig. 2, may enter the permanent pycnocline; the remaining part will return to the mixed layer during the subsequent mixed layer entrainment period.

The period of detrainment can, thus, be divided into two phases. The first phase is the effective detrainment: during this period, water from the mixed layer passes through the seasonal pycnocline and eventually enters the permanent pycnocline. The amount of detrainment during the effective detrainment period is defined as the annual mean subduction rate. The second phase is the ineffective detrainment period, in which water from the mixed layer enters the seasonal pycnocline and is subsequently reentrained into the mixed layer downstream.

Entrainment dominates in subpolar basins. Like during the ineffective detrainment period, water entrained into the mixed layer may not actually originate from the permanent pycnocline; instead, it may be the water

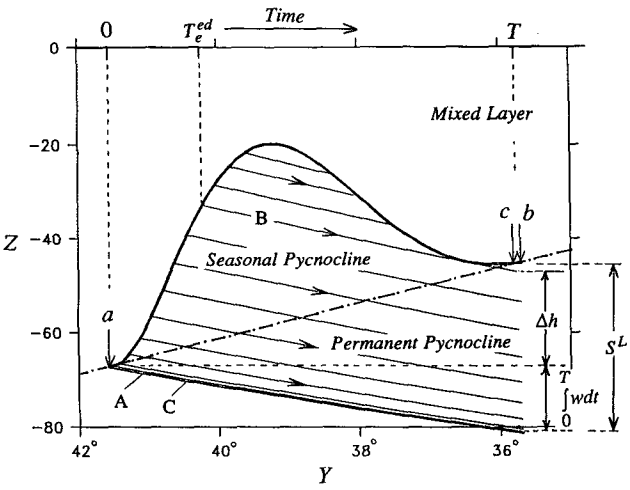

FIG. 2. A conceptual model of subduction. The upper ocean is divided into three layers: the mixed layer on the top, the permanent pycnocline below the annual maximum depth of the mixed layer, and the seasonal pycnocline in-between. Downward-pointing arrows denote along-isopycnal, geostrophic flows, which are continuous across the seasonal and permanent pycnoclines. Abscissa indicates the southward trajectory of a particle as the time passes on.

previously detrained out of the mixed layer (Woods 1985; Cushman-Roisin 1987). In order to clarify the physical processes involved in entrainment, we introduce the term *obduction* to describe the process in which water from the permanent pycnocline is transferred into the overlying seasonal pycnocline and eventually enters the mixed layer above. The term obduction has been used in geology to describe the process of upward thrusting of a crustal plate over the margin of an adjacent plate. It is worth mentioning that the now familiar term *subduction* was also borrowed from geology. Obduction, as it is defined, is the result of effective entrainment that occurs only during a part of the entrainment period (see Fig. 3). During the rest of the entrainment period, water entering the mixed layer has been exposed to air–sea interactions over the past year.

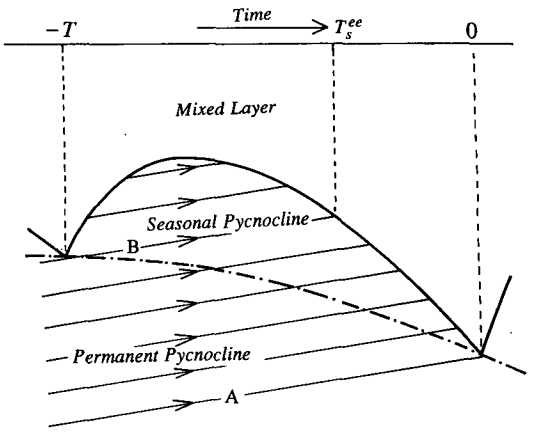

FIG. 3. Same as Fig. 2 except for the conceptual model of obduction.

Using the special term, obduction, helps us in describing the irreversible mass flux from the permanent pycnocline to the mixed layer. For example, although mixed layer entrainment takes place in the subtropical basins over a long period in the seasonal cycle, water entrained into the mixed layer in most places is actually the water detrained into the seasonal pycnocline in the past year, suggesting no effective entrainment, or no obduction. In fact, obduction takes place only within the subpolar basins and the subtropical–subpolar boundary regions, as will be shown through processing the climatological data in this study.

Though an antonym of subduction, obduction is not simply subduction with an opposite sign. They are different in many ways. First, the physical processes involved in subduction and obduction are different. Subduction takes place largely in subtropical basins, where water flows geostrophically into the permanent pycnocline from above. As a result, the subducted water entering the permanent pycnocline carries the temperature and salinity determined by the mixed layer processes, and these properties are essentially conserved during the motion after subduction. Obduction, however, takes place mainly in subpolar basins, where water flows geostrophically and upward from the underlying permanent pycnocline. As this water enters the mixed layer, it quickly loses its identity due to convective mixing, and it is impossible to keep track of the trajectory of an individual water particle thereafter.

This difference in physics is also reflected in the mathematical formulation of suitable boundary value problems for the climatological mean pycnocline structure in the subtropical and subpolar basins (Huang 1988). The pycnocline equation is a nonlinear hyperbolic equation. In the subtropical basin, density is specified as an upper boundary condition because the base of the mixed layer is the upstream boundary. In the subpolar basin, on the other hand, the upper surface density cannot be specified. In fact, the mixed layer density is determined by the dynamics of the permanent pycnocline, which is a part of the solution. The introduction of seasonal boundary layer physics requires a reformulation of the boundary conditions for the theories of the pycnocline structure in the subtropical and subpolar basins. Coupling the seasonal mixed layer with the permanent pycnocline into simple analytical models, however, remains a challenge.

The second major difference between subduction and obduction is the time when effective detrainment and effective entrainment occur. It is well known that effective detrainment takes place after late winter when the mixed layer reaches its annual maximum depth and starts to retreat. By contrast, effective entrainment takes place between late fall and early winter when the mixed layer deepens quickly but has not yet reached its maximum depth and density.

Third, for the annual mean subduction rate calculation, one follows the trajectories of water particles downstream for one year to ascertain whether they go into the permanent pycnocline (Woods 1985). In calculating the annual mean obduction rate, on the other hand, one has to trace back to the origin of the entrained water in order to make sure that it actually originates from the permanent pycnocline.

An important application of the subduction/obduction rate is the determination of the average age of water masses, which can be compared to the tracer age obtained through geochemical tracer studies. Water mass age or tracer age not only provide insight into the circulation physics, they are also useful for inferring the ocean circulation's temporal variability. At the base of the mixed layer, water masses are formed by subduction and destroyed by obduction. A rough estimation of the renewal time for a particular water mass can be made by dividing the subduction (obduction) rate by the water mass volume. These two estimates, however, need not be equal because diapycnal mixing and mass exchange through lateral boundaries, such as the southern boundary of our single-hemisphere model, can also contribute to the water mass formation/con-

version. A minimum of these two estimates can be used as a useful indicator of the water mass renewal time.

In this study, the subduction and obduction rates in the North Atlantic and the North Pacific are calculated using the available climatological datasets. The term *ventilation* is used to indicate the water mass exchange between the permanent pycnocline and the seasonal pycnocline; it can be either subduction or obduction. Our calculation of the ventilation rate is based on a simple formula defined in Lagrangian coordinates, as discussed in section 2. This approach is applied to both the North Atlantic and the North Pacific in sections 3 and 4. The results reflect the distinctive differences in the thermohaline circulation and the mixed layer dynamics in these two oceans, as discussed in section 5.

2. The subduction/obduction rate

Although detrainment occurs during a substantial period of the seasonal cycle, water subducted into the permanent pycnocline is strongly biased toward the late winter properties due to the rapid shoaling of the mixed layer in early spring (Stommel 1979). The effective detrainment period diagnosed from climatological data is rather short, about 1–2 months, for most of the North Atlantic subtropical basin (Marshall et al. 1993). Therefore, the subduction rate based on the winter mixed layer properties, as first suggested by Stommel (1979, the Stommel demon), provides a good approximation to the annual mass flux from the mixed layer to the permanent pycnocline.

The instant detrainment rate in three-dimensional mixed layer models is defined as (e.g., De Szoeke 1980; Cushman-Roisin 1987)

$$D = -\left(w_{mb} + \mathbf{u}_{mb}\cdot\nabla h_m + \frac{\partial h_m}{\partial t}\right), \qquad (1)$$

where w_{mb} and $\mathbf{u}_{mb}$ are the vertical and horizontal velocities at the base of the mixed layer, and h_m is the depth of the mixed layer. Since only the effective detrainment contributes to subduction, the annual mean subduction rate in Eulerian coordinates is

$$S_{\text{ann}} = \frac{1}{T}\int_{T_s^{ed}}^{T_e^{ed}} D\,dt, \qquad (2)$$

where $T = 1$ year and T_s^{ed} and T_e^{ed} are the times when effective detrainment starts and ends, which are determined by tracing trajectories of particles (released at the base of the mixed layer) downstream for one year.

Cushman-Roisin (1987) also discussed obduction in Eulerian coordinates briefly, wherein he called it "entrainment of deep water." Similar to Eq. (2), the annual mean obduction rate in Eulerian coordinates is

$$O_{\text{ann}} = -\frac{1}{T}\int_{T_s^{ee}}^{T_e^{ee}} D\,dt, \qquad (3)$$

where T_s^{ee} and T_e^{ee} are the times when effective entrainment starts and ends, which are determined by tracing the trajectories upstream for one year. The advantage of using Eulerian coordinates is that the subduction/obduction rate is clearly defined at each station. Use of Eulerian coordinates, however, requires detailed information about the seasonal cycle, upon which defining the effective detrainment/entrainment period depends.

The annual mean subduction rate can also be defined in Lagrangian coordinates (see Woods 1985):

$$S_{\text{ann}} = -\frac{1}{T}\int_0^T w_{tr}\,dt - \frac{1}{T}\int_0^T \mathbf{u}_{tr}\cdot\nabla h_m\,dt, \qquad (4)$$

where the integration is taken along the first effective subducted trajectory starting typically from March of the first year and ending in March of the second year. In Eq. (4), w_{tr} and $\mathbf{u}_{tr}$ are the vertical and horizontal velocities along the trajectory. The first term in Eq. (4) represents the contribution from vertical pumping at the base of the mixed layer, and the second term the contribution from lateral induction due to the slope of the mixed layer base. Equation (4) has been used by Woods (1985) to estimate the ventilation rate diagnostically from the monthly climatological data of Robinson et al. (1979). Woods and Barkmann (1986) have further estimated the ventilation rate prognosticly by Lagrangian integration of a mixed layer model driven by surface fluxes. Using numerical results from a general circulation model, Williams et al. (1994) have determined the seasonal cycle and the subduction rate and period in the North Atlantic.

In this study we propose that it is not necessary to resolve the entire seasonal cycle if one is only interested in diagnosing the annual mean subduction (obduction) rate. To avoid resolving the entire seasonal cycle, we will use a simplified version of Eq. (4) in defining the annual mean subduction rate:

$$S_{\text{ann}} = -\overline{\left(w_{\text{Ek}} - \frac{\beta}{f}\int_{-h_m}^{0} v\,dz\right)} + \frac{1}{T}(h_{m,0} - h_{m,1}), \qquad (5)$$

where w_{Ek} is the Ekman pumping velocity, which can be estimated from wind stress data, and the β term denotes the vertical velocity reduction due to the meridional velocity in the surface layer. The overbar indicates an average over the one-year Lagrangian trajectory, and $h_{m,0}$ and $h_{m,1}$ indicate the mixed layer depths in the first and second March, respectively. Notice that because the Ekman layer is much shallower than the winter mixed layer, the vertical pumping velocity at the base of the winter mixed layer is generally smaller than the Ekman pumping velocity in subtropical regions.

The physical interpretation of Eq. (5) is illustrated in Fig. 2; it shows an idealized case simulating subduction taking place along a meridional section. To highlight the physics, the annual maximum depth of the mixed layer is assumed to be a linear function of

latitude, as indicated by the dotted–dashed line. In addition, we assume the mixed layer depth to have a simple sinusoidal seasonal cycle. The exact Lagrangian subduction rate is calculated by following a particle released at station a at the time when the effective detrainment starts ($T_s^{ed} = -0.0244$ in this case, with one year equal to one unit in time and $t = 0$ corresponding to Mach 1); its corresponding trajectory in Fig. 2 is labeled as A. At regular time intervals, water particles detrained into the pycnocline are monitored and their downstream trajectories followed. Not all these particles can enter the permanent pycnocline. As seen in Fig. 2, trajectory B indicates the boundary between effective and ineffective detrainment; that is, water detrained later than T_e^{ed} will be overtaken by mixed layer entrainment at a downstream location. The annual mean subduction rate in Fig. 2 is equal to the vertical distance between the two trajectories A and B at the end of one year (at station b),

$$S_{\text{ann}} = \int_0^T w dt + \Delta h.$$

Although this calculation is straightforward, it requires detailed information about the seasonal cycle of the mixed layer, which is usually ill-resolved by the climatological datasets.

Our simplified definition of (5) substitutes the mixed layer depth at T_s^{ed} by the maximum depth in winter. Instead of starting the trajectory at $t = -0.0244$, the particle is launched at $t = 0$, and the annual mean subduction rate S^L is given by the vertical distance between trajectory C and the March mixed layer depth at station c. As indicated in Fig. 2, the difference between these two subduction rates is rather small. Since the seasonal cycle of the mixed layer depth in the real ocean has a saw-tooth profile, the sharp change in the winter mixed layer depth tends to further reduce the difference between the two definitions. Notice that other sources of error also exist in calculating the annual mean subduction (obduction) rate. For example, the Levitus dataset has only seasonal salinity values; this introduces an error in computing the March mixed layer properties. Compared with these error sources, we expect the error introduced in our simplified definition to be insignificant.

Similar to Eq. (5), the annual mean obduction rate in Lagrangian coordinates can be simplified to

$$O_{\text{ann}} = \overline{\left(w_{\text{Ek}} - \frac{\beta}{f}\int_{-h_m}^{0} v dz\right)} + \frac{1}{T}(h_{m,0} - h_{m,-1}), \quad (6)$$

where $h_{m,0}$ is the mixed layer depth in the present winter, and $h_{m,-1}$ is the mixed layer depth in the previous winter. The difference in sign between Eq. (5) and Eq. (6) reflects the downstream/upstream tracing approaches in detecting the effective detrainment/entrainment trajectories.

Figure 3 illustrates the physical processes involved in obduction (see Woods 1985). As we noted above, obduction calculation requires upstream tracing of water particles from the current winter at $t = 0$ to the previous winter at $t = -T$. After the water from the permanent pycnocline flows geostrophically into the seasonal pycnocline, it eventually enters the mixed layer in late fall and early winter. As shown in Fig. 3, water entrained into the mixed layer before T_s^{ee} does not originate from the permanent pycnocline; it is the mixed layer water detrained to the seasonal pycnocline at an upstream location. Note that a saw-tooth type of mixed layer depth cycle has been assumed in this case, so that the difference between the trajectory grazing the base of the mixed layer in the current and previous winters and the trajectory starting from the base of the mixed layer on 1 March becomes indiscernible.

It is worth noting that the subduction/obduction rates calculated in Eulerian or Lagrangian coordinates should always be nonnegative because they are defined only for the effectively detrained/entrained waters. A negative rate of subduction (obduction) obtained by the simplified definition (5) or (6) in Lagrangian coordinates is meaningless. It only implies that no effectively detrained (entrained) trajectories exist. In such a case, the annual mean subduction (obduction) rate should be zero.

It is intuitive here to examine the ventilation rate at the place where the Kuroshio (or the Gulf Stream) separates from the western boundary. A prominent maximum in the late winter mixed layer depth exists off the coast of Japan due to strong cooling of cold, dry polar air from the continent (see Fig. 9b). For simplicity, we assume that the alongcurrent-path distribution of the late winter mixed layer depth can be represented by the profile shown in Fig. 4a. Also assume the seasonal cycle of the mixed layer depth, $f(t)$, has the typical saw-tooth profile shown in Fig. 4b (the thin line). The mixed layer depth pattern in this case becomes

$$h_m(x, t) = h_{\min} + [100(1 + 0.001x) + 100e^{-(x/\Delta x)^2} - h_{\min}]f(t), \quad (7)$$

where $h_{\min} = 40$ m is the mixed layer depth minimum and Δx is the width of the Cauchy profile.

Where the Kuroshio separates from the coast water travels relatively fast, which combined with the strong mixed layer depth gradient, makes a large contribution to the ventilation rate. In comparison, the contribution to ventilation due to Ekman pumping is negligible because this is close to the intergyre boundary. For this intuitive example, we will neglect the vertical pumping and assume water parcels travel 1000 km within one year. Our focus is on the station at the center of the winter mixed layer trough, $x = 0$. The instantaneous Eulerian subduction/obduction rate calculated using Eq. (1) is shown in Fig. 4b by the thick line. Effective detrainment begins at $t = 0$ (1 March) when the mixed

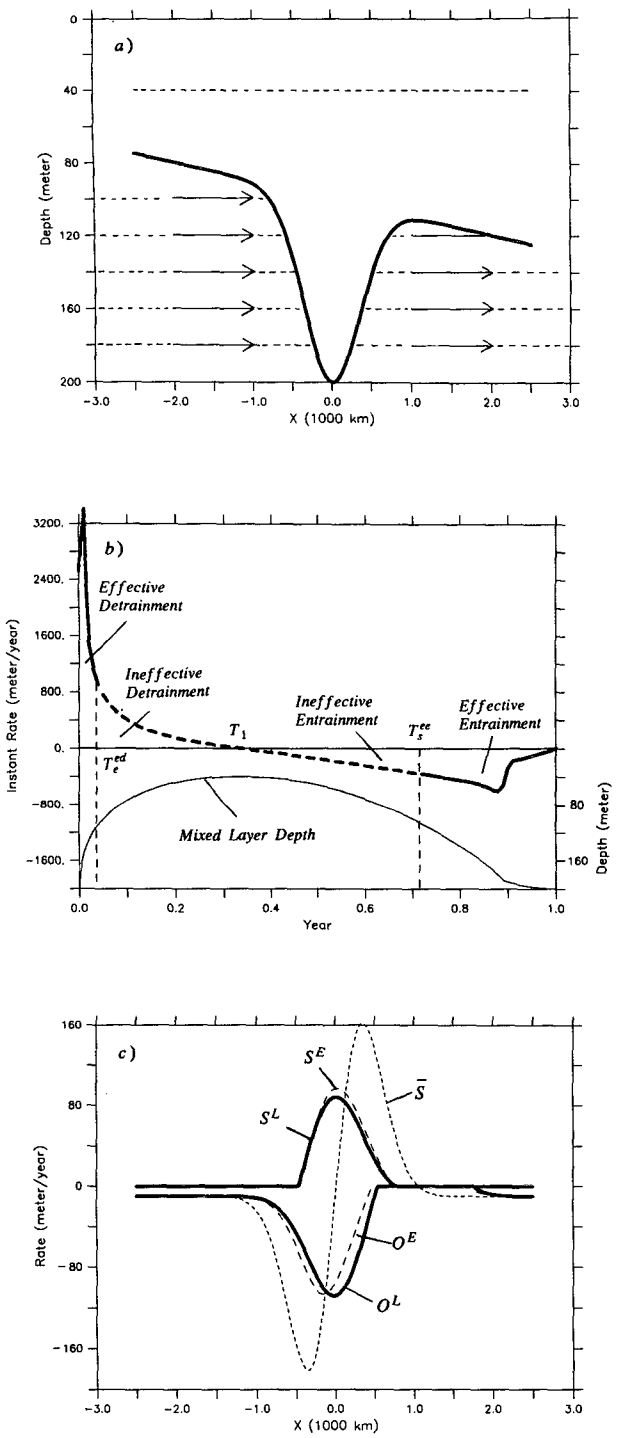

FIG. 4. An intuitive example of ventilation taking place along the path of the Kuroshio Extension. (a) Mixed layer depth in late winter (solid curve) and in summer (dashed line). Trajectories of water particles are depicted by horizontal arrows. (b) Instantaneous detrainment/entrainment rate at station $x = 0$ as a function of time. The thin solid line indicates the seasonal cycle of the local mixed layer depth. (c) Annual mean subduction (positive) and obduction (negative) rates: heavy solid lines indicate the Lagrangian rates, long-dashed lines the Eulerian rates, and the short-dashed line is the rate calculated using the local winter mixed slope as defined in Eq. (8).

layer starts to shoal rapidly. The end of the effective detrainment, $T_e^{ed} = 0.037$, is determined by tracing water particles released from this station regularly at a time interval of $\Delta t = 0.001$. The ineffective detrainment period is between T_e^{ed} and $T_1 = 0.336$ because the water subducted during this period is entrained into the downstream mixed layer at a later time. Entrainment starts at T_1. The beginning of the effective entrainment is determined by tracing water particles upstream for one year. It occurs in this case at $T_s^{ee} = 0.716$. Notice that although detainment takes place for one-third of the year, the duration of the effective detrainment is rather short, about 13 days. Similarly, entrainment takes place during the remaining two-thirds of the year, but only the last half of this period, about 103 days, is effective entrainment.

At $x = 0$ as shown in Fig. 4b, effective entrainment takes place in winter. Near the end of winter, entrainment slows down and is eventually overtaken by detrainment. Since the transition between these two processes is relatively quick, water obducted into the mixed layer remains close to the location where it leaves the permanent pycnocline. During the rapid mixed layer shoaling in spring, this same water is left behind and it flows geostrophically into the permanent pycnocline thereafter. Thus, obduction and subduction can take place at the same location in different phases of the seasonal cycle.

The spatial distribution of the annual mean ventilation rates are shown in Fig. 4c, in which the subduction rate is defined as positive and the obduction rate is defined as negative. The solid lines denote the rates calculated in Lagrangian coordinates [Eqs. (5) and (6)], while the long-dashed lines denote those calculated in Eulerian coordinates [Eqs. (2) and (3)]. Not surprisingly, the subduction/obduction rates calculated using these two formulas agree well both in magnitude and in spatial distributions. A small difference arises because the two definitions use different weighting on the annual means. Four dynamically distinctive regions appear in Fig. 4c. In the upstream, there is a region of pure obduction because the mixed layer depth increases monotonously downstream. In the middle of the mixed layer depth trough there is an ambiductive region where both subduction and obduction take place and compensate for each other. There is a narrow band downstream, where only subduction occurs. Farther downstream, an insulated region exists where neither subduction nor obduction occurs.

For comparison, the subduction/obduction rate calculated using just the annual mean velocity and winter mixed layer depth,

$$\bar{S} = -\bar{\mathbf{u}} \cdot \nabla h_{\text{winter}} \tag{8}$$

(Woods 1985) is shown in Fig. 4c by the short-dashed line. Such a formula is similar to the one used by Marshall et al. (1993) in their data analysis of subduction for the North Atlantic and by Huang and Russell

(1994) in their analytical study for the subtropical North Pacific. This definition represents the annual mass flux across unit area at the upper surface of the permanent pycnocline. In comparison, the definition we used in this study represents the annual net effective detrainment/entrainment across the base of the mixed layer. Obviously, these two definitions are different because they are defined at different control surfaces. As shown in Fig. 4c, definition (8) inflates the subduction/obduction rate near the mixed layer depth fronts. In addition, such a definition eliminates possible overlapping and exclusion of subduction and obduction because it neglects the seasonal cycle and the along-trajectory changes.

In the following, the Lagrangian definition for ventilation is applied to the North Atlantic and the North Pacific. The annual mean subduction/obduction rates in these two oceans are calculated according to the following steps:

1) The mixed layer depth and density for March are based on the Levitus climatology, where the mixed layer density is calculated using March temperature and winter salinity data, and the mixed layer depth is defined as the depth at which σ_θ differs by 0.125 from the surface σ_θ.

2) The along-isopycnal horizontal velocities are calculated from the annual Levitus climatology by integrating the thermal wind equations from a reference level of 2000 m. This reference level was shown by Roemmich and McCallister (1989) to be adequate for the North Pacific and it also appears to be appropriate for the North Atlantic (Rintoul and Wunsch 1991). To obtain the horizontal velocity on a given isopycnal surface, we first computed the acceleration potential by integrating the density anomaly from the reference level; namely,

$$A = p_0\delta_0 + \int_{\delta_0}^{\delta} p\,d\delta, \tag{9}$$

where p_0 is the reference pressure, δ the specific volume anomaly, and δ_0 the specific volume anomaly at the reference pressure (Montgomery and Stroup 1962). The along-isopycnal geostrophic velocities are estimated from the acceleration potential as follows:

$$-2\Omega \sin\phi v = -\frac{1}{a\cos\phi}\frac{\partial A}{\partial \lambda} \tag{10}$$

$$2\Omega \cos\phi u = -\frac{1}{a}\frac{\partial A}{\partial \phi}, \tag{11}$$

where a is the radius of the earth, ϕ is latitude, λ is longitude, and Ω is the rotation rate of the earth. Trajectories of water particles released from the base of the March mixed layer are then calculated accordingly.

3) The annual mean Ekman pumping velocity is estimated using the Hellerman and Rosenstein (1983, hereafter HR) wind stress data. There has been concern about the drag coefficients used in the HR calculation. Harrison (1989) and Trenberth et al. (1990) pointed out that the HR wind stress is about 20%–30% higher than the results from a more accurate bulk formula used by Large and Pond (1981): the maximum barotropic streamfunction in the subtropical North Pacific, for example, is 62 Sv (Sv $\equiv 10^6$ m^3 s^{-1}) from the HR data, but it is about 50 Sv according to the new wind stress data by Trenberth et al. In the following analysis, we used the HR wind stress data reduced by a factor of 0.8. In this case, the maximum barotropic streamfunctions for the North Atlantic and North Pacific subtropical gyres are 28 and 50 Sv, agreeing with the result by Trenberth et al. (1990).

3. Ventilation of the North Atlantic

Figure 5a shows the density at the base of the March mixed layer in the North Atlantic. Note that this density communicates with the permanent pycnocline and is $0.125\sigma_\theta$ heavier than the density at the surface. The weak meridional density gradient σ_θ between 26.2 and 26.4 located south of the Gulf Stream corresponds to the site of the subtropical mode water formation.

The depth of the March mixed layer is shallow, about 50 m, along the southern rim of the North Atlantic subtropical basin but becomes increasingly deeper toward higher latitudes (Fig. 5b). The maximum mixed layer depth exceeds 1000 m in the Labrador Sea and between Greenland and Iceland. Because the monthly Levitus data are only available for the upper 1000 meters and the potential density referred to the sea surface is not very accurate for such a large depth change, we have put an artificial limit of 1000 m on the mixed layer depth. Around the British Isles and Iceland, small areas exist where the mixed layer extends to the ocean floor (see crosses in Fig. 5b); these areas are not included in the following analysis. A remarkable feature in Fig. 5b is the existence of a trough of mixed layer depth maximum extending all the way from south of Georges Bank to the British Isles. This trough is due to the strong atmospheric cooling over the path of the warm and salty North Atlantic Current (NAC). The impact of this trough on the ventilation rate will be discussed in detail shortly.

The annual mean Ekman pumping rate calculated from the scaled HR data is shown in Fig. 6a. Downwelling dominates in the subtropical basin; its magnitude varies from 0 along the intergyre boundary to −60 m/yr along the southern rim of the subtropical basin. In the subpolar basin, upwelling prevails increasing from 0 near the intergyre boundary to 60 m/yr near Greenland.

Figure 6b shows the one-year trajectories of particles released at the base of the March mixed layer (small crosses indicate starting points). As discussed in section 2, the subduction rate is calculated by following

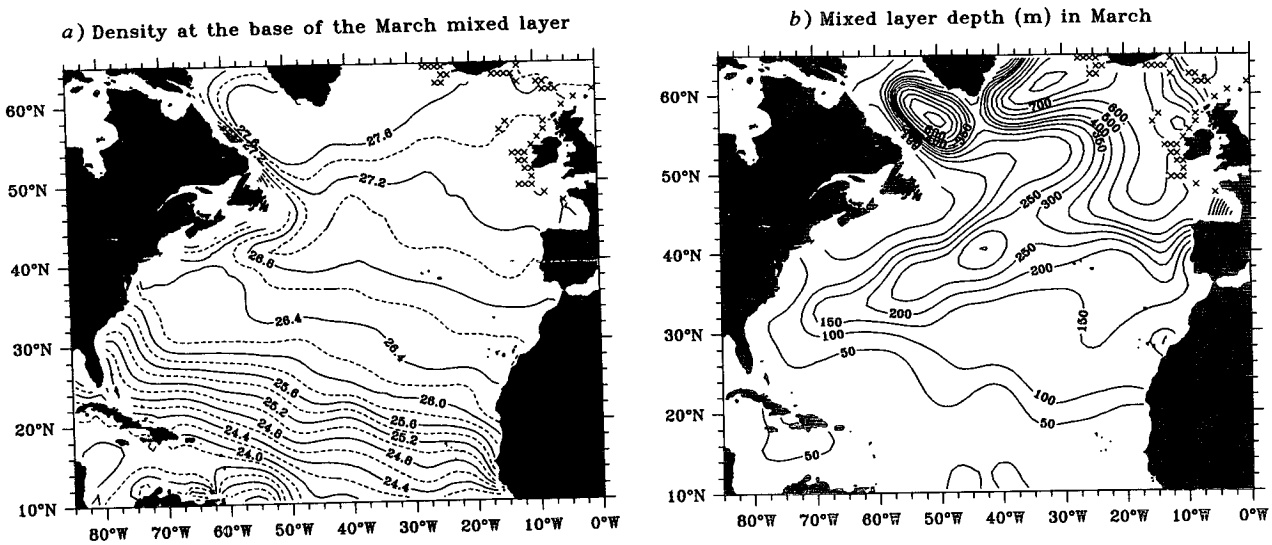

FIG. 5. (a) Density in σ_θ and (b) depth in meters of the March mixed layer in the North Atlantic. Based on the Levitus (1982) March temperature and winter salinity data.

these trajectories. To calculate the obduction rate, however, one has to trace the particles upstream for one year. These upstream trajectories are not shown in Fig. 6b in order to avoid confusion.

Ventilation rates for the North Atlantic are shown in Fig. 7. To make the discussion complete we have included the maps for subduction and its two constituent terms. Marshall et al. (1993) have estimated the subduction rates for the North Atlantic based on the Isemer and Hasse (1987) annual mean wind stress dataset, which is slightly different from the HR dataset. The subduction rate from our calculation is smaller than that found by Marshall et al. For example, the maximum subduction rate south of the Gulf Stream extension region within $\sigma_\theta = 26.0$–26.8 (Fig. 5a) is about 100 m/yr in this study, as compared to 150 m/yr from their calculation. This difference is due to the different definitions for the annual mean subduction rate used in the two studies. As we noted in the previous section, using the simple definition of Eq. (8) tends to inflate the annual mean ventilation rate near the mixed layer depth fronts (see Fig. 4c). In Fig. 7c, there are two isolated locations in the subpolar basin where localized subductions take place. (These two localized subductions

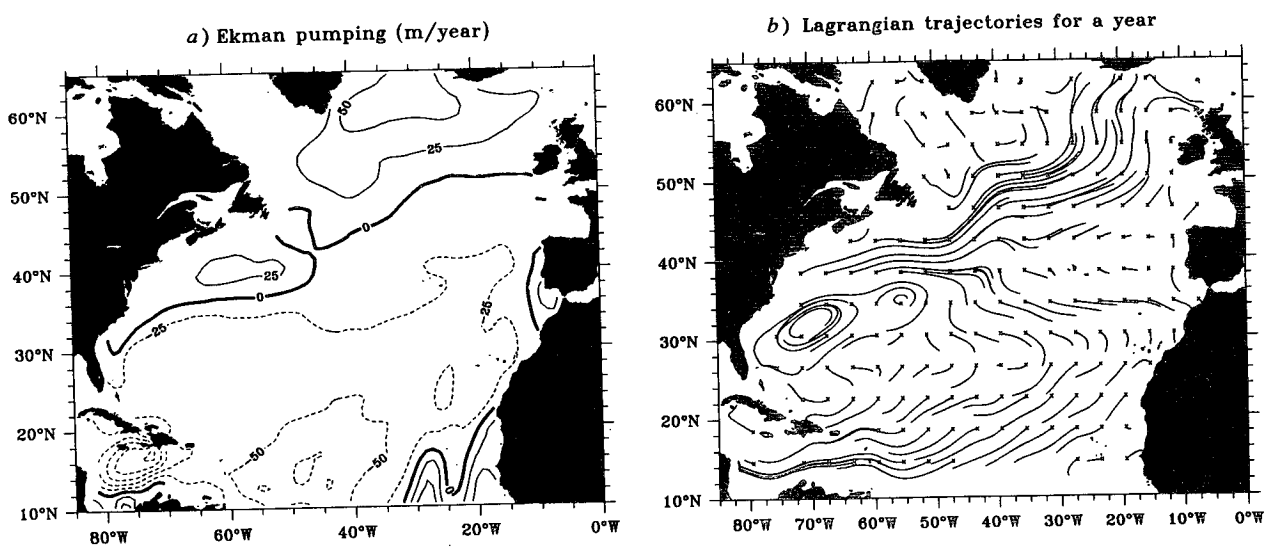

FIG. 6. (a) Ekman pumping rate in the North Atlantic, in m/yr, based on the scaled HR (1983) data. (b) One-year trajectories of water particles in the North Atlantic released from the base of the March mixed layer. The along-isopycnal geostrophic velocities are calculated using the 2000-m depth as the reference level.

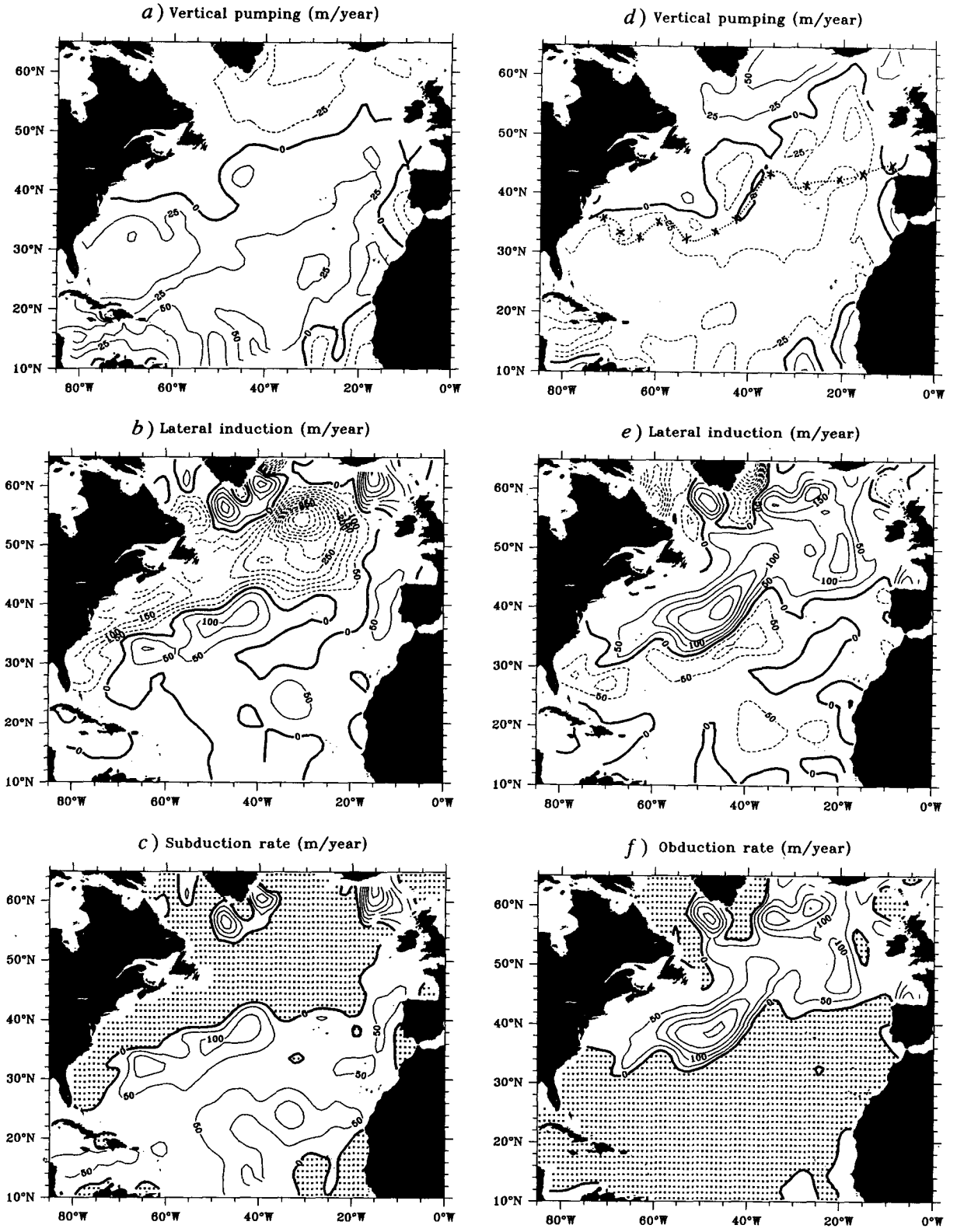

FIG. 7. Annual mean ventilation rate for the North Atlantic. Subduction rate and its two components are shown in (a) the vertical pumping term, (b) the lateral induction term, and (c) the subduction rate. Stippled regions in (c) indicate zero subduction rate. Obduction rate and its two components are shown in (d) the vertical pumping term, (e) the lateral induction term, and (f) the obduction rate. Stippled regions in (f) indicate zero obduction rate. The dotted line with crosses in (d) indicates the southern limit of the obduction zone.

TABLE 1. Ventilation rates for the North Atlantic and the North Pacific in Sverdrups (10^6 m^3 s^{-1}).

	North Atlantic	North Pacific	Sum
(A) Subduction			
Ekman pumping	(−22.2)	(−30.8)	(−53.0)
Vertical pumping	17.5	25.1	42.6
Lateral induction	9.5	10.1	19.6
Total subduction	27.0 + 3.1[a]	35.2	65.3
(B) Obduction			
Ekman pumping	(2.8)	(3.6)	(6.4)
Vertical pumping	−0.62	3.1	2.5
Lateral induction	24.1	4.7	28.8
Total obduction	23.5	7.8	31.3
(C) Local conversion	4.0	3.5	7.5

[a] 3.1 Sv is the sum of localized subduction south of Iceland (1.9 Sv) and in the Labrador Sea (1.2 Sv).

are also seen in the map by Marshall et al. 1993.) The total amount of subduction is 1.9 Sv south of Iceland and 1.2 Sv south of Greenland.

The obduction rate also includes contributions from the vertical pumping term and the lateral induction term. It is readily seen from Fig. 7d that the vertical pumping pattern for obduction is slightly different from that of subduction seen in Fig. 7a. The lateral induction pattern, Fig. 7e, is entirely different from its corresponding pattern for subduction shown in Fig. 7b. The sum of these two terms gives the annual mean obduction rate, Fig. 7f. The annual mean obduction rate reaches a maximum, about 250 m yr^{-1}, along the paths of the Gulf Stream and the NAC in the density range of σ_θ = 26.6–27.2. For these geographical locations, Marshall et al. (1993) obtained a negative subduction rate of more than 350 m/yr. In the interior subpolar gyre, their maximum is above 300 m/yr, which is much larger than 200 m/yr estimated from our calculation. These larger ventilation rates are again the result of using the crude formula [Eq. (8)], which exaggerates the contribution of the mixed layer depth gradient. In most of the subtropical basin, the obduction rate is zero because the water entering the mixed layer during the entrainment phase (in fall) is the water that was detrained to the seasonal pycnocline somewhere upstream, not from the permanent pycnocline.

The total mass flux partition for the North Atlantic is shown in the left column of Table 1. Within the subtropical basin, the total amount of subduction is 27.0 Sv, to which vertical pumping contributes 17.5 Sv and lateral induction contributes 9.5 Sv. In comparison, Huang (1990) estimated the total subduction rate in the North Atlantic to be 24.8 Sv, with 12.1 Sv from vertical pumping and 12.7 Sv from lateral induction. The larger value for the vertical pumping term from this study is due to the inclusion of the domain down to 10°N, where the Ekman pumping rate is large. Note that the total vertical pumping rate across the base of the annual maximum depth of the mixed layer (17.5 Sv) is smaller than the total Ekman pumping rate across the base of the Ekman layer (22.2 Sv). This difference reflects the reduction of vertical velocity due to the southward motion in the mixed layer, as indicated by the second term on the right-hand side of Eq. (5).

The total obduction rate (23.5 Sv) is one order of magnitude larger than the Ekman pumping rate and is dictated by lateral induction (24.1 Sv), with a very small negative contribution from the vertical pumping term. The fact that vertical pumping makes a negative contribution to obduction is interesting and unexpected. To understand this result, we divide the domain of obduction into three regions; the mass flux partitions within each of these regions are listed in Table 2. Region I is defined by where the Ekman pumping is positive, so it makes a positive contribution to the total obduction rate. Since water in the mixed layer moves northward in this region (Fig. 6), vertical pumping is substantially reduced from 4.1 Sv at the base of the Ekman layer to 1.7 Sv at the base of the winter mixed layer.

In region II, the Ekman pumping velocity is downward and the meridional velocity in the mixed layer is southward (see Fig. 6). As a result, vertical pumping is slightly increased from −0.72 Sv at the base of the Ekman layer to −0.67 Sv at the base of the winter mixed layer. In region III, Ekman pumping velocity is again downward, but the meridional velocity is now poleward (Fig. 6b). This reduces the vertical pumping rate from −0.6 Sv at the base of the Ekman layer to −1.6 Sv at the base of the winter mixed layer. As a result, the net contribution to the obduction rate over the North Atlantic from vertical pumping is negative (−0.6 Sv), a value much smaller than the contribution from lateral induction (24.1 Sv).

The strong obduction in the North Atlantic is closely related to the thermohaline circulation in the basin. Because of the deep-water formation in the Norwegian–Greenland Sea, the warm and salty water of the Gulf Stream is drawn into the subpolar basin in the form of the North Atlantic Current, a part of the well-known conveyor belt in the North Atlantic. Over a large part

TABLE 2. Mass flux partitions within the obduction region in the North Atlantic, in Sverdrups (10^6 m^3 s^{-1}). Note: The calculation covers stations north of 30°N.

	Region I $w_e > 0$	Region II $w_e < 0$ South of 40°N	Region III $w_e < 0$ North of 40°N	Sum
Ekman pumping	(4.1)	(−0.72)	(−0.57)	(2.8)
Vertical pumping	1.7	−0.67	−1.6	−0.6
Lateral induction	13.2	4.1	6.7	24.1
Total obduction	14.9	3.4	5.2	23.5

of the subpolar North Atlantic, the heat transported by the NAC is released to the atmosphere, as can be seen in Fig. 8 by the relatively large heat flux values (>60 W m^{-2}) from ocean to atmosphere. Excessive evaporation along the path of the NAC is associated with this heat loss (e.g., Schmitt et al. 1989). The combination of strong cooling and high salinity due to evaporation gives rise to an outstanding trough in the winter mixed layer depth that extends from south of Georges Bank to the British Isles (Fig. 5b). The combination of the fast-flowing NAC and the large depth gradient in the winter mixed layer result in a strong lateral induction, which dominates the obduction rate in the subpolar North Atlantic.

Since the subduction and obduction processes in this study are defined according to their different physics, we now have new situations that would not have appeared if the definition of Eq. (8) were used. In addition to the regions of pure subduction and pure obduction, there are now ambiductive regions where both subduction and obduction take place (see the contoured regions in Fig. 8) and insulated regions where neither subduction nor obduction takes place (the shaded regions in Fig. 8).

In the region of the Gulf Stream extension, the mixed layer depth reaches its local maximum in late winter due to strong atmospheric cooling (see the dashed contours in Fig. 8). In this region, lateral induction is large for both subduction and obduction. Starting from the local mixed layer maximum and tracing the particle upstream for a year, the rapid decline in the mixed layer depth gives rise to a large obduction rate as shown in Fig. 7f. Similarly, following the particle downstream for a year gives a large subduction rate (Fig. 7c) due again to the mixed layer depth declining along the trajectories. As we noted from the example shown in Fig. 4, the ambiductive regions are characterized by a strong seasonal cycle; in these regions, effective entrainment takes place in late fall and early winter when the mixed layer steadily deepens, while subduction takes over in late winter and spring when the mixed layer rapidly retreats. To quantify this dual process, we calculated the local conversion rate, defined as the minimum of the annual mean subduction and obduction rate. This rate is shown by the solid contours in Fig. 8; the total amount of the local conversion rate is 3.1 Sv.

It is worth noting that the local conversion is not a pure kinematic process. On the contrary, mixed layer properties change substantially between the effective entrainment phase and the effective detrainment phase. This is readily seen from the heat flux contours superimposed on Fig. 8 that the ambiductive region of the Gulf Stream extension is very closely correlated with the region where the atmospheric cooling is strongest.

The ambiductive spot south of Greenland can be identified as the site of Labrador Sea Water formation (McCartney and Talley 1982; Killworth 1983). The total amount of subduction in this region is 1.2 Sv and

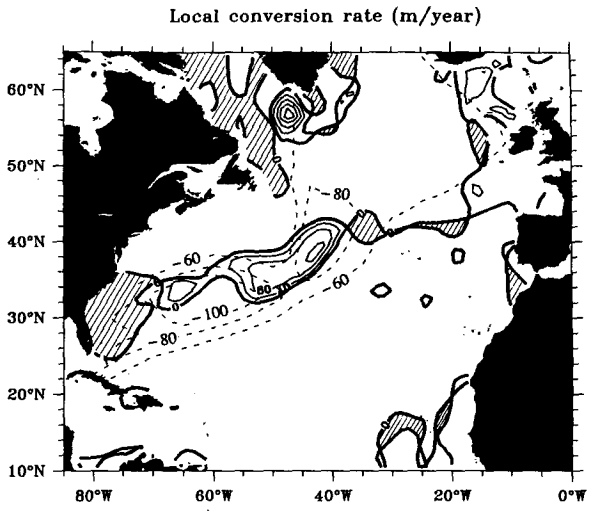

FIG. 8. Local mass conversion rate in the North Atlantic, defined within the ambiductive region, with contour interval of 40 m/yr. The shaded areas are insulated regions where neither subduction nor obduction takes place. The dashed lines indicate the annual heat loss from the ocean to the atmosphere, in units of W m^{-2}, adapted from Hsiung (1985).

the total conversion rate is 0.51 Sv. These numbers are well below the estimated rate for Labrador Sea Water formation of about 3.1 Sv by Clarke and Gascard (1983) and 10 Sv by McCartney and Talley (1984). This discrepancy is probably due to the limitation of the Levitus data in this region because the Labrador Sea Water formation can occur on a length scale of just a few hundred kilometers (Clarke and Gascard 1983), too short to be resolved by the highly smoothed Levitus dataset. Rather than claiming these numbers, we hope that our calculation demonstrates the physical processes involved in this area and that the exact numbers will be obtained in the future when more accurate datasets become available.

South of Iceland, there is a third ambiductive region in our calculation, where the total subduction rate is 1.9 Sv and the total conversion rate is 0.37 Sv. No previous studies have indicated any significant water mass formation in this region; the source region of deep-water formation is located to the north in the middle of the Norwegian–Greenland Sea (Killworth 1983). Thus, this feature is probably an artifact due to limitation of existing data in this area.

The existence of insulated regions is an interesting phenomenon; they appear where the March mixed layer depth is locally minimum. For example, the March mixed layer is very shallow near the western boundary (Fig. 5b); since this is near the recirculation region, one-year trajectories either downstream or upstream end where the March mixed layer is deeper. As a result, the lateral induction term is negative in both subduction and obduction calculations (Figs. 7b and 7e), and no effective ventilation occurs within this region.

4. Ventilation of the North Pacific

Figure 9a shows the density at the base of the March mixed layer in the North Pacific. Compared with the North Atlantic, the meridional density gradient north of 30°N in Fig. 9a is much stronger, reflecting that the North Pacific is dominated by freshwater flux forcing. The March mixed layer depth in the North Pacific (Fig. 9b) is quite shallow compared with the North Atlantic. In fact, the maximum depth of the mixed layer near the Kuroshio Extension is only about 175 m. In most of the subpolar basin, the mixed layer depth gradually decreases from its maximum of 175 m to about 100 m near the eastern boundary. The mixed layer depth maximum near the Kuroshio Extension is associated with strong atmospheric cooling along the path of the warm current. The shallow mixed layer in the subpolar basin reflects the fact that the subpolar North Pacific is dominated by an excess of precipitation over evaporation. As a result, a strong halocline develops in the upper ocean, preventing convective mixing from giving rise to a deep winter mixed layer.

Figure 10a shows the Ekman pumping rate in the North Pacific calculated from the scaled HR data. This pattern is not much different from that in the North Atlantic, except that upwelling in the subpolar basin is weaker: the maximum Ekman pumping rate in the subpolar North Pacific is about 25 m/yr, as compared to 65 m/yr in the North Atlantic. In both basins, the zero-Ekman-pumping lines are tilted in the SW–NE orientation. A closer inspection, however, reveals that this tilt is 50% larger in the North Atlantic than it is in the North Pacific. To a certain degree, the slope of the zero-Ekman-pumping line reflects the strength of the poleward heat flux carried by the ocean. In the North Atlantic, the poleward heat flux is larger. As a result, the surface water is warmer along the path of the NAC, so that the wind stress pattern is altered by the warm current as discussed by Behringer et al. (1979). In the North Pacific, there is no such warm current across the intergyre boundary, resulting in a smaller slope of the zero-Ekman-pumping line. Trajectories of water particles released from the base of the March mixed layer are depicted in Fig. 10b. As we have noted above, the major difference between the trajectories in the North Pacific and the North Atlantic (Fig. 6b) is the absence of a fast current, like the NAC, across the intergyre boundary in the North Pacific.

The annual mean subduction and obduction rates are shown in Fig. 11. The subduction maps are essentially the same as those of Huang and Qiu (1994); these maps are included to complete the discussion. Our focus is again on the obduction maps. Figure 11d shows the contribution from the vertical pumping term and Fig. 11e, the lateral induction term. There is a positive contribution from lateral induction along the Kuroshio Extension path and in the northwestern part of the subpolar basin because of the large change in the mixed layer depth. In the northeastern part of the basin, the lateral induction rate is mostly negative, and the total obduction rate (Fig. 11f) is more or less determined by the vertical pumping rate. The obduction rate reaches a maximum of 75 m/yr off the Japan coast, a result due to the strong lateral induction associated with the large gradient of the winter mixed layer depth. A second obduction maximum of 75 m/yr is located in the vicinity of the Bering Abyssal Plain, which is due to the combination of the lateral induction and vertical pumping terms.

As in the North Atlantic, ambiductive and insulated regions also exist in the North Pacific, as shown in Fig. 12. The largest ambiductive region, which has a local

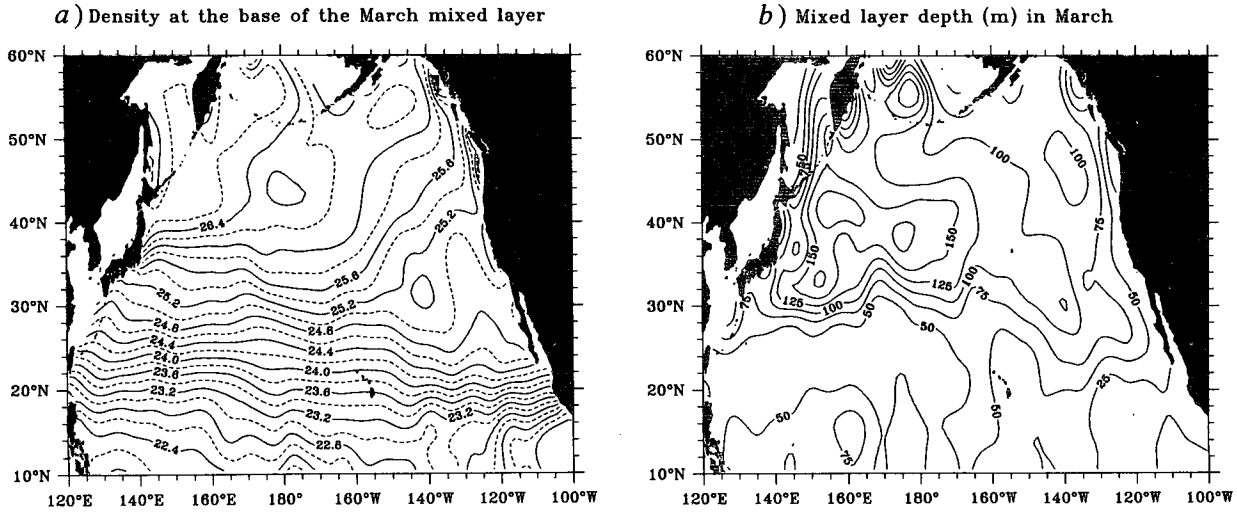

FIG. 9. (a) Density in σ_θ and (b) depth in meters of the March mixed layer in the North Pacific. Based on the Levitus (1982) March temperature and winter salinity data.

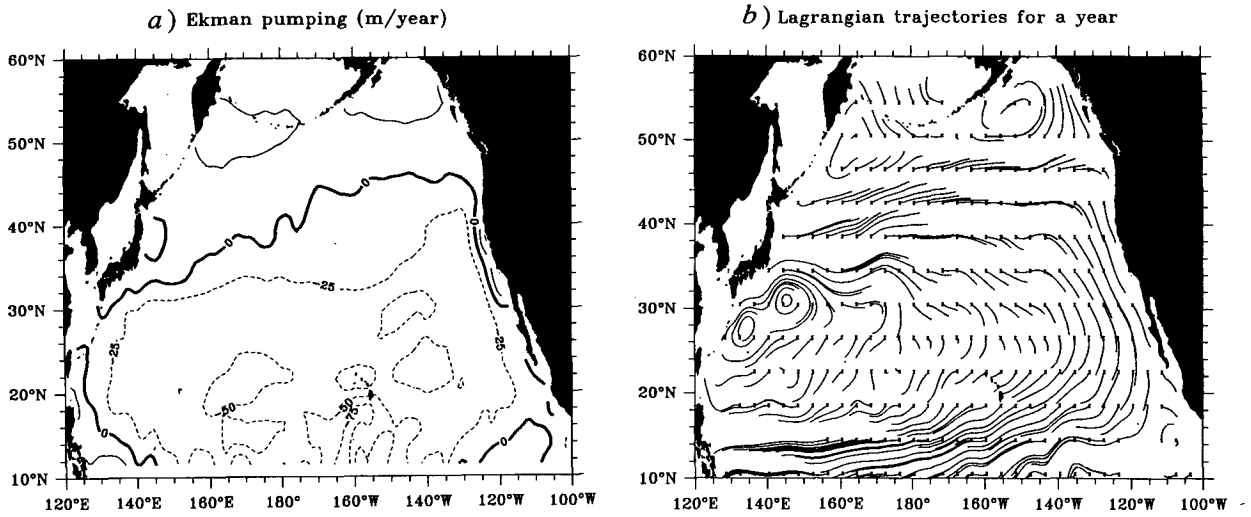

FIG. 10. (a) Ekman pumping rate in the North Pacific, in m/yr, based on the scaled HR (1983) data. (b) One-year trajectories of water particles in the North Pacific released from the base of the March mixed layer. The along-isopycnal geostrophic velocities are calculated using the 2000-m depth as the reference level.

conversion rate of up to 75 m/yr, is located in the Kuroshio Extension region. This ambiductive region is again coincident with the location of the strongest heat loss from the ocean to the atmosphere, as indicated by the dashed contours in Fig. 12. A small ambiductive region, with a local conversion rate of about 25 m/yr, can also be seen near the Bering Abyssal Plain.

The basin-integrated subduction rate in the North Pacific is 35.2 Sv, including 25.1 Sv from vertical pumping and 10.1 Sv from lateral induction. These numbers are slightly different from those (33.1 Sv, 24.1 Sv, and 9.0 Sv) presented by Huang and Qiu (1994); the discrepancy is due to the different areas used in the summation. The total obduction rate in the North Pacific is 7.8 Sv, including 3.1 Sv from vertical pumping and 4.7 Sv from lateral induction. The total local conversion rate is 3.5 Sv, about the same as that in the North Atlantic.

5. Discussion

The purpose of the present study is to explore ventilation in the Northern Hemisphere oceans. Subduction in the subtropical basins has been discussed in many previous studies. In comparison, obduction has received much less attention. We have focused on obduction in this study by first clarifying the similarities and differences between the subductive and obductive processes. Second, we analyzed the available climatological data and estimated the subduction/obduction rate in the North Atlantic and North Pacific. Because the definition for obduction requires tracing water particles upstream for one year, the results are different from those obtained by tracing the particles downstream for one year, a commonly used method for estimating the subduction rate in the subtropical basins. One of the new features emerging from our calculation is the existence of ambiductive and insulated regions in oceans.

The ambiductive regions, where both subduction and obduction occur, appear mainly along the paths of the Gulf Stream and the Kuroshio Extension, and they are closely associated with the maximum heat loss from the ocean to the atmosphere. In these regions, rapid mixed layer deepening in winter gives rise to a large mass flux from the permanent pycnocline to the mixed layer. In late winter, the process switches to the subduction mode. By analyzing an idealized model and the climatological data, we demonstrated that these two processes may take place at the same location, but at different phases of the seasonal cycle.

Notice that although the total subduction rates in the North Atlantic and the North Pacific are comparable (30.1 Sv vs 35.2 Sv), the characteristics of water masses being annually subducted into the permanent pycnoclines are quite different. As indicated in Fig. 13, subduction in the North Atlantic transfers higher density water into the pycnocline than in the North Pacific. The transfer has two peaks in the North Atlantic. The peak around 26.2–26.6 σ_θ corresponds to the formation of the subtropical mode water (STMM), which is known for its large volume and uniform properties near 18°C and 36.5 psu (Worthington 1976). The total formation rate for STMW, if defined between 26.0 and 27.0 σ_θ, is 13.3 Sv (Table 3) in this study. This rate agrees well with the value of 14.1 Sv by Woods and Barkmann (1986), who estimated the annual rate of STMW formation by using a mixed layer model forced by surface heat flux and Ekman pumping.

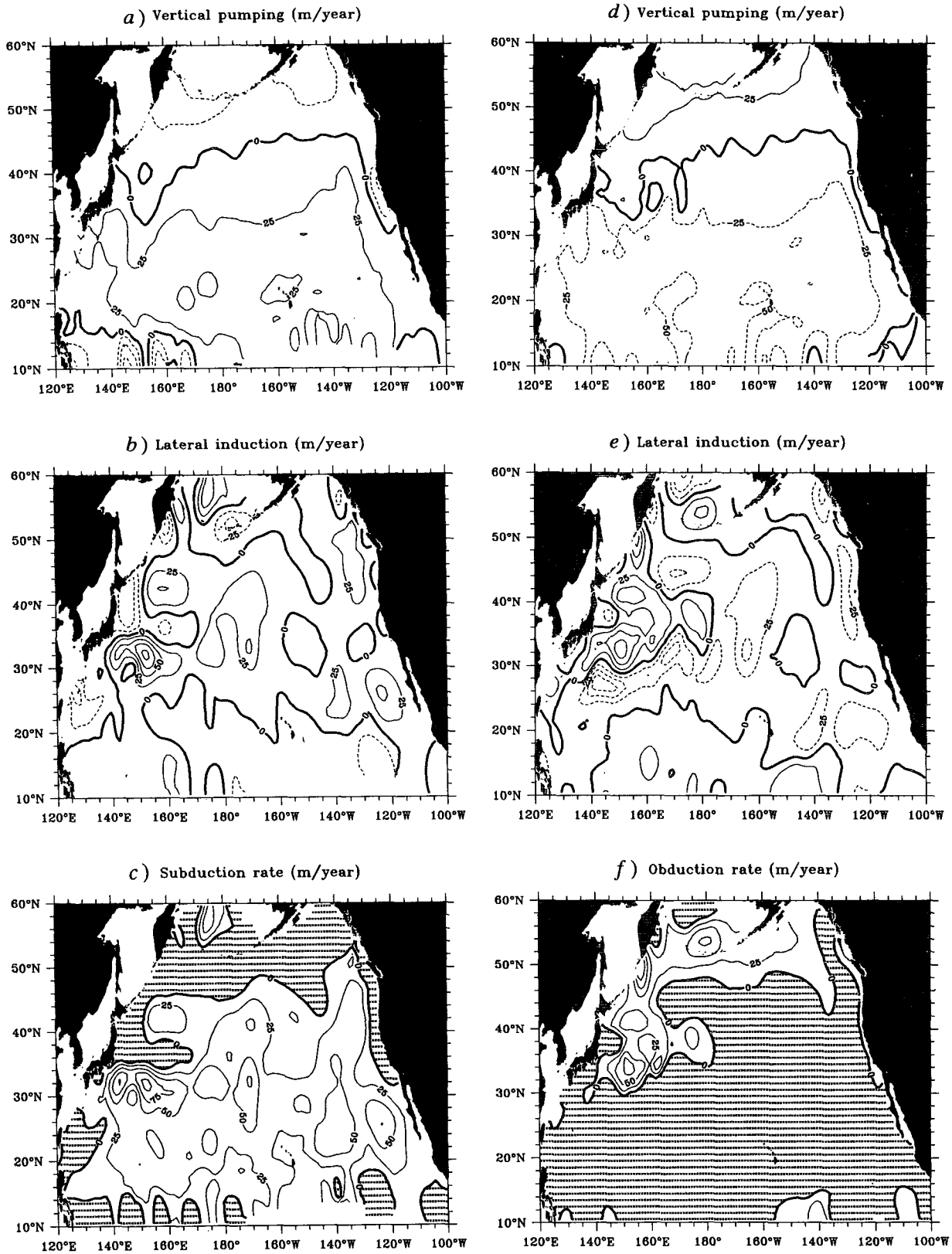

FIG. 11. Annual mean ventilation rate for the North Pacific. Subduction rate and its two components are shown in (a) the vertical pumping term, (b) the lateral induction term, and (c) the subduction rate. Stippled regions in (c) indicate zero subduction rate. Obduction rate and its two components are shown in (d) the vertical pumping term, (e) the lateral induction term, and (f) the obduction rate. Stippled regions in (f) indicate zero obduction rate.

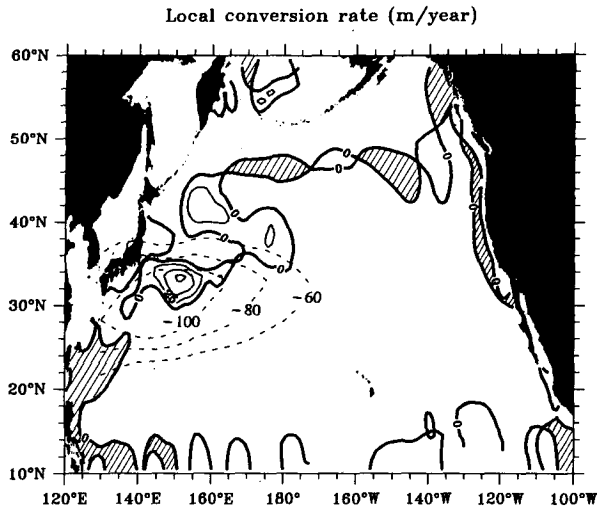

FIG. 12. Local mass conversion rate in the North Atlantic, defined within the ambiductive region, with contour interval of 25 m/yr. The shaded areas are insulated regions where neither subduction nor obduction takes place. The dashed lines indicate the annual heat loss from the ocean to the atmosphere, in units of W m^{-2}, adapted from Hsiung (1985).

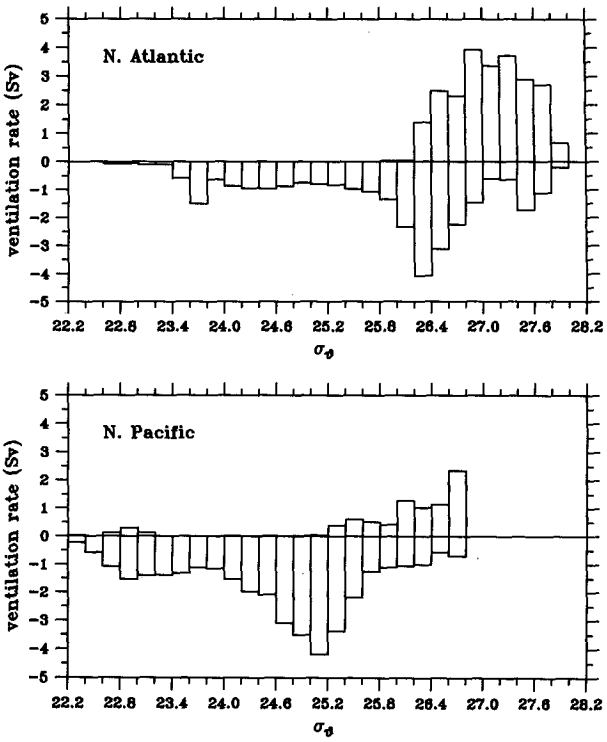

FIG. 13. Subduction/obduction rates per 0.2 σ_θ interval as a function of density for the North Atlantic (upper) and the North Pacific (lower).

Speer and Tziperman (1992) also calculated the water mass formation rate. Their calculation was based on surface heat and freshwater flux data, without considering the dynamic processes within the mixed layer nor the exchange between the mixed layer and the permanent pycnocline. The major difference between their calculation and ours is that only part of the water mass formed at the surface can penetrate into the permanent pycnocline, and this portion corresponds to the subduction rate calculated in our study. In addition, they gave only a single water mass formation (destruction) rate for a given density range, while our calculation provides both the water formation rate due to subduction and the water mass destruction rate due to obduction. Nevertheless, the water mass formation rate of 14 Sv over the density range between 26.0 and 27.0 derived by Speer and Tziperman is close to our estimation.

The second subduction peak in Fig. 13a corresponds to the formation of subpolar mode water, or Labrador Sea Water (McCartney and Talley 1982). The formation rate for subpolar mode water, as we discussed in section 3, is likely underestimated due to the limitation of the Levitus data. In the North Atlantic, the obduction rate peaks between 26.8 and 27.4 σ_θ, where the subduction rate is locally minimum. This result is consistent with the observations that an oxygen minimum exists around 27.2 σ_θ in the North Atlantic (Richards and Redfield 1955).

In addition to the subduction rate, which indicates how much new water is pumped into the permanent pycnocline, we have also calculated the obduction rate, which indicates how fast water in the permanent pycnocline is returned to the mixed layer after cycling through the ocean's interior. For the North Atlantic, the total obduction rate between 26.0 and 27.0 σ_θ is 10.1 Sv. Thus, there is a net gain of 3.2 Sv for this density range; this net gain is probably balanced by cross-isopycnal mixing and flows across the southern boundary (10°N). Similarly, for the density range from 27.0 to 28.0 σ_θ the total amount of subduction is 4.3 Sv, the total obduction is 13.3 Sv, and the difference of −9 Sv

TABLE 3. Water mass conversion rates for the North Atlantic and the North Pacific, in SV (10^6 m^3 s^{-1}).

	Density in σ_θ					
	22–23	23–24	24–25	25–26	26–27	27–28
			(a) North Atlantic			
Due to subduction		2.9	4.4	5.0	13.3	4.3
Due to obduction		/		−0.03	−10.1	−13.3
Net conversion		2.9	4.4	5.0	3.2	−9.0
			(b) North Pacific			
Due to subduction	1.9	6.1	12.2	12.1	3.3	
Due to obduction			−0.1	−2.0	−5.8	
Net conversion	1.9	6.1	12.1	10.1	−2.5	

should be balanced by cross-isopycnal mixing and flows across the southern boundary.

In the North Pacific (Fig. 13b), the single subduction peak around 25.0–25.2 σ_θ corresponds to the formation of North Pacific subtropical mode water. The North Pacific STMW has typical water properties of 16.5°C and 34.75 psu (Masuzawa 1969; Suga et al. 1989), and it is clear that the freshness of the North Pacific is responsible for the lighter density of the subducted waters. The annual formation rate for the North Pacific STMW, if defined between 24.8 and 25.6 σ_θ, is 13.2 Sv. There exists no counterpart for subpolar mode water in the North Pacific, a manifestation of the difference in the thermohaline circulation between the two oceans, as we emphasized above.

Notice that with the exception of the heaviest isopycnal layers with σ_θ = 26.0–26.8, most isopycnal layers in the North Pacific gain a large volume of mass flux through subduction because of weak obduction. The total, excessive mass flux is about 27.7 Sv (see Table 3). Since the thermohaline circulation is weak in the North Pacific, most of this mass flux should leave the domain of calculation through the southern boundary (10°N). In fact, Huang and Qiu (1994) estimated the total southward mass flux across 15°N to be about 19.3 Sv.

Given both subduction and obduction rates, two renewal timescales may be defined. For the North Atlantic STMW (σ_θ = 26.0–27.0), renewal times based on the subduction and obduction rates are shown in Table 4 in the first and second rows, respectively. In the lighter density range, the renewal time is shorter due to subduction, whereas in the denser density range, the renewal time is shorter due to obduction. Since other processes, such as diapycnal mixing, also contribute to the water mass renewal, the smaller value of the two is a more appropriate scale for the renewal time. According to Table 4, the renewal time for the North Atlantic STMW ranges from 10 to 30 years.

The large difference in obduction between the North Atlantic and the North Pacific is attributable to the difference in the thermohaline circulation in these two oceans. In the North Atlantic, deep-water formation occurs in the Norwegian–Greenland Sea. This deep-water source drives an energetic meridional overturning in the North Atlantic. As a result, the permanent pycnocline in the North Atlantic is renewed on a relatively short time scale. In the present study, the rapid ventilation of the subpolar North Atlantic is reflected by the large value of the obduction rate, 23.5 Sv, which represents the total amount of water being transferred from the permanent pycnocline into the mixed layer annually. In comparison, the total amount of obduction in the North Pacific is only 7.8 Sv, about one-third of that in the North Atlantic.

One way of quantitatively estimating the difference in the thermohaline circulation in these two oceans is to look at the time required to renew a water mass that outcrops in the subpolar basins. If we ignore the effects due to diapycnal mixing and water mass exchange through the southern boundaries (10°N), the renewal time for the water mass of σ_θ = 27.0–27.2 in the subpolar North Atlantic is 46 years and that of σ_θ = 27.2–27.4 is 71 years. Beyond σ_θ = 27.4, the renewal time can exceed 100 years, but these numbers are less reliable, because of the questionable quality of the data used in estimating the obduction rate (see section 3). In the subpolar North Pacific, the renewal time is longer in general: about 80 years for the water mass of σ_θ = 26.2–26.4 and 96 years for that of σ_θ = 26.4–26.6. It is well known that there is no deep-water formation in the North Pacific (Warren 1983), and the global thermohaline circulation is driven by deep-water sources in the North Atlantic and the bottom-water source in the Weddell Sea. Since these sources are remote, the thermohaline circulation in the North Pacific is weak and the subpolar water mass renewal rate is likely to be small. These notions are consistent with the above estimations.

The difference in the thermohaline circulation is also reflected in the properties of the mixed layer. In the North Atlantic, deep-water formation in the Norwegian–Greenland Sea induces a strong cross-gyre North Atlantic Current, which transports warm and salty water from the subtropical basin all the way to the British Isles. This warm current gives rise to more evaporation and hence less salinity stratification in the upper layer. As winter comes, heat loss to the atmosphere creates a very deep mixed layer along the path of the North Atlantic Current. The large horizontal gradient in the mixed layer depth along the NAC's path, in turn, gives rise to a large value for lateral induction, which is the dominant contributor to the obduction rate in the subpolar North Atlantic.

In contrast, there is no strong warm current across the boundary of the subtropical and the subpolar gyres

TABLE 4. Water mass renewal time for the North Atlantic subtropical mode water, in years.

	Density in σ_θ				
	26.0–26.2	26.2–26.4	26.4–26.6	26.6–26.8	26.8–27.0
Due to subduction	16.0	11.4	18.0	33.7	74.0
Due to obduction	1016.1	33.8	22.6	32.9	27.9

in the North Pacific because of the weak thermohaline circulation. The surface temperature in the subpolar basin is low, limiting the amount of evaporation. As a consequence, precipitation exceeds evaporation and a strong, shallow halocline develops over most of the subpolar basin. This strong stratification near the surface prevents deep convection and limits the heat loss from the ocean to the atmosphere. Thus, the mixed layer in most of the subpolar North Pacific is more or less uniform and no deeper than 125 m. The small mixed layer depth gradient is directly responsible for the small obduction rate there.

Finally, we note that our calculation is based on the Levitus (1982) dataset. The possible poor quality of this dataset at high latitudes raises questions about the accuracy of our calculated maps. Although some details may be inaccurate, we believe that the global structure of ventilation in these maps is appropriate. As high quality in-situ data rapidly accumulate from the on-going, various observational programs, our estimation of the ventilation of the World Ocean will undoubtedly improve.

Acknowledgments. This study benefited from many discussions with Dennis Moore, Joe Pedlosky, Roger Samelson, and Bruce Warren. Reviewers carefully read earlier versions of our manuscript and provided many constructive comments. In particular, John Woods offered many critical comments that forced us to clarify the terminology and interpretation of our results. B.Q. was supported by the National Science Foundation through Grant OCE94-03048. R.X.H. was partially funded by Cooperative Agreement No. NA 37RJ0199 from the National Oceanic and Atmospheric Administration at the University of Hawaii. He was also supported by the National Science Foundation through Grant OCE93-00706 to the Woods Hole Oceanographic Institution.

REFERENCES

Behringer, D., L. Regier, and H. Stommel, 1979: Thermal feedback as a contributing cause of the Gulf Stream. *J. Mar. Res.*, **37,** 699–709.

Clarke, R. A., and J.-C. Gascard, 1983: The formation of Labrador Sea Water. Part I: Large-scale processes. *J. Phys. Oceanogr.*, **13,** 1764–1778.

Cushman-Roisin, B., 1987: Subduction. *Dynamics of the Oceanic Surface Mixed Layer.* P. Muller and D. Henderson, Eds., Hawaii Inst. of Geophysics Special Publications, 181–196.

De Szoeke, R. A., 1980: On the effects of horizontal variability of wind stress on the dynamics of the ocean mixed layer. *J. Phys. Oceanogr.*, **10,** 1439–1454.

Harrison, D. E., 1989: On climatological mean wind stress and wind stress curl fields over the World Ocean. *J. Climate,* **2,** 57–70.

Hellerman, S., and M. Rosenstein, 1983: Normal monthly wind stress over the world ocean with error estimates. *J. Phys. Oceanogr.*, **13,** 1093–1104.

Hsiung, J., 1985: Estimates of global oceanic meridional heat transport. *J. Phys. Oceanogr.*, **15,** 1405–1413.

Huang, R. X., 1988: On boundary value problems of the ideal-fluid pycnocline. *J. Phys. Oceanogr.*, **18,** 619–641.

——, 1990: On the three-dimensional structure of the wind-driven circulation in the North Atlantic. *Dyn. Atmos. Oceans,* **15,** 117–159.

——, and B. Qiu, 1994: Three-dimensional structure of the wind-driven circulation in the subtropical North Pacific. *J. Phys. Oceanogr.*, **24,** 1608–1622.

——, and S. Russell, 1994: Ventilation of the subtropical North Pacific. *J. Phys. Oceanogr.*, **24,** 2589–2605.

Iselin, C. O. D., 1939: The influence of vertical and lateral turbulence on the characteristics of the waters at mid-depths. *Trans. Amer. Geophys. Union,* **20,** 414–417.

Isemer, H. J., and L. Hasse, 1987: *The Bunker Climate Atlas of the North Atlantic Ocean,* Vol. 2. Springer-Verlag, 252 pp.

Killworth, P. D., 1983: Deep convection in the World Ocean. *Rev. Geophys. Space Phys.*, **21,** 1–26.

Large, W. G., and S. Pond, 1981: Open ocean momentum flux measurements in moderate to strong winds. *J. Phys. Oceanogr.*, **11,** 324–336.

Levitus, S., 1982: *Climatological Atlas of the World Ocean.* NOAA Prof. Paper No. 13, U.S. Govt. Printing Office, Washington, DC, 173 pp.

Marshall, J. C., A. J. G. Nurser, and R. G. Williams, 1993: Inferring the subduction rate and period over the North Atlantic. *J. Phys. Oceanogr.*, **23,** 1315–1329.

Masuzawa, J., 1969: Subtropical mode water. *Deep-Sea Res.*, **16,** 463–472.

McCartney, M. S., and L. D. Talley, 1982: The subtropical mode water of the North Atlantic Ocean. *J. Phys. Oceanogr.*, **12,** 1169–1188.

——, and ——, 1984: Warm-to-cold water conversion in the northern North Atlantic Ocean. *J. Phys. Oceanogr.*, **14,** 922–935.

Montgomery, R. B., and E. D. Stroup, 1962: Equatorial waters and currents at 150°W in July-August 1952. *John Hopkins Oceanographic Studies,* No. 1, 68 pp.

Richards, F. A., and A. C. Redfield, 1955: Oxygen-density relationships in the western North Atlantic Ocean. *Deep-Sea Res.*, **2,** 182–189.

Rintoul, S. R., and C. Wunsch, 1991: Mass, heat, oxygen and nutrient fluxes and budgets in the North Atlantic Ocean. *Deep-Sea Res.*, **38**(Suppl.), 355–377.

Robinson, M. K., R. A. Bauer, and E. H. Schroeder, 1979: Atlas of North Atlantic—Indian Ocean monthly mean temperatures and mean salinities of the surface layers. U.S. Naval Oceanogr. Office Ref. Publ. 18, Washington, DC, 194 pp.

Roemmich, D., and T. McCallister, 1989: Large scale circulation of the North Pacific Ocean. *Progress in Oceanography,* Vol. 22, Pergamon, 171–204.

Schmitt, R. W., P. S. Bogden, and C. E. Dorman, 1989: Evaporation minus precipitation and density fluxes for the North Atlantic. *J. Phys. Oceanogr.*, **19,** 1208–1221.

Speer, K., and E. Tziperman, 1992: Rates of water mass formation in the North Atlantic Ocean. *J. Phys. Oceanogr.*, **22,** 93–104.

Stommel, H. M., 1979: Determination of water mass properties of water pumped down from the Ekman layer to the geostrophic flow below. *Proc. Natl. Acad. Sci., USA,* **76,** 3051–3055.

Suga, T., K. Hanawa, and Y. Toba, 1989: Subtropical mode water on the 137°E section. *J. Phys. Oceanogr.*, **19,** 1605–1618.

Trenberth, K. E., W. G. Large, and J. G. Olson, 1990: The mean annual cycle in global ocean wind stress. *J. Phys. Oceanogr.*, **20,** 1742–1760.

Warren, B. A., 1983: Why is no deep water formed in the North Pacific? *J. Mar. Res.*, **41,** 327–347.

Williams, R. G., M. A. Spall, and J. C. Marshall, 1994: Does Stommel's mixed-layer "demon" work? *J. Phys. Oceanogr.*, in press.

Woods, J. D., 1985: The physics of pycnocline ventilation. *Coupled Ocean–Atmosphere Models.* J. C. J. Nihoul, Ed., Elsevier Sci. Pub., 543–590.

——, and W. Barkmann, 1986: A Lagrangian mixed layer model of Atlantic 18°C water formation. *Nature,* **319,** 574–576.

Worthington, L. V., 1976: On the North Atlantic circulation. *John Hopkins Oceanographic Studies,* No. 6, 110 pp.